energy&fuels

Article

Cite This: Energy Fuels XXXX, XXX, XXX−XXX

pubs.acs.org/EF

Vanadyl Porphyrin Speciation Based on Submegahertz Ligand Proton Hyperfine Couplings

Donald Mannikko and Stefan Stoll*

Department of Chemistry, University of Washington, Seattle, Washington 98195, Unites States

ABSTRACT: The speciation of vanadyl (VO^{2+}) porphyrins in crude oil (vanadyl petroporphyrins) is an area of ongoing interest in petroleomics. In this paper, we describe a method for the speciation of vanadyl porphyrins that uses electron nuclear double resonance (ENDOR), a high-resolution electron paramagnetic resonance (EPR) spectroscopic technique. We use ^{1}H ENDOR to measure hyperfine couplings between ligand protons and the paramagnetic vanadyl ion as small as about 0.15 MHz. From the measured hyperfine couplings, we directly determine all vanadium−ligand proton distances up to 8 Å. This information differentiates porphyrin ligands by their ring substitution pattern and substituent nature. We demonstrate this using a series of vanadyl porphyrin model compounds. Additionally, we demonstrate that the composition of binary vanadyl porphyrins mixtures can be determined. The ability of ENDOR to differentiate types of ligand protons in vanadyl porphyrin mixtures provides a basis for analyzing more complex mixtures of vanadyl petroporphyrins.

INTRODUCTION

The petroleum industry refines billions of barrels of crude oil annually. An important step in crude oil refining is catalytic hydrotreating. This removes or deactivates contaminants that interfere with further processing or the burning of fuel.[1] Unfortunately, in the process of hydrotreating, catalysts are deactivated by a buildup of coke and metal deposition.[2−4] The deposition of vanadium is particularly problematic; quantities of vanadium as low as 2% of the total mass built up on the catalyst can result in a 50% loss in catalytic activity.[1,5] Therefore, there is great interest in the removal of vanadium from crude oil.[5−17]

The separation of vanadium compounds from crude oil is nontrivial since the majority of vanadium compounds reside in asphaltene and bitumen (paraffinic layers of crude oil that form aggregates in many solvents).[18,19] The concentration of vanadium in petroleum varies geographically, from $\lesssim$10 ppm to $\gtrsim$1200 ppm.[9,11] A better understanding of vanadium compounds in crude oil could lead to improved separation techniques.[20] Speciation of the vanadium compounds in crude oil is challenging due to the difficulty of chemical separation; however, there has been success in determining information about the nature of vanadium in asphaltenes and unprocessed crude oil.[16]

X-ray spectroscopy reveals that essentially all the vanadium in crude oil is in the form of vanadyl ions (VO^{2+}, consisting of V^{4+} and O^{2-}) coordinated to porphyrin ligands via four nitrogens.[21] The most common technique in contemporary petroleomics is Fourier transform ion cyclotron resonance mass spectrometry (FT-ICR MS). Through FT-ICR MS, hundreds of different petroporphyrins have been resolved; the most common petroporphyrins include octaethylporphyrin (OEP), etioporphyrin (EP), and deoxophylloerythroetioporphyrin (DPEP).[6,22] In FT-ICR MS, porphyrins are characterized by their molecular formula and grouped into series according to their heteroatom content.[23]

Developing alternative methods for speciation may be useful with respect to the analysis of vanadyl porphyrins. Such methods need to satisfy two primary requirements: (1) The method should be able to work with minimal processing or separation to preserve the integrity of the sample and chemical identities in the sample. (2) The method should have a resolution high enough to differentiate chemically similar vanadyl porphyrins.

Electron paramagnetic resonance (EPR) spectroscopy meets the above requirements. EPR detects only paramagnetic moieties. Therefore, most of the compounds present in an unrefined sample of oil will be invisible to EPR. The vanadyl ion, VO^{2+}, however, is paramagnetic, with total electron spin 1/2. In addition, the EPR spectra of vanadyl compounds are different and consequently distinguishable from other paramagnetic species present in crude oils, such as organic free radicals and Mn^{2+}.[11] Therefore, measurements can be made with little to no separation. A small sample of crude oil can be directly placed in an EPR sample tube. This meets the first requirement listed above. As we show in this paper, the high-resolution requirement can be achieved by pulse EPR techniques, which have resolving power on the order of ≈0.1 MHz.

EPR has long been used to investigate crude oil.[14,24−26] A continuous-wave (CW) EPR method has been used to quantify the total amount of vanadyl in crude oil.[11] Higher-resolution EPR experiments have also been useful. Electron nuclear double resonance (ENDOR) spectroscopy has been used to examine the hyperfine coupling of vanadyl compounds including porphyrins.[27−29] Recently, ^{1}H ENDOR has been combined with density functional theory (DFT) to compare calculated proton hyperfine couplings with experimental petroporphyrin measurements.[13]

In this paper, we use high-resolution ^{1}H ENDOR spectroscopy to measure model vanadyl porphyrin compounds. We

Received: March 20, 2019
Revised: April 23, 2019
Published: April 24, 2019

DOI: 10.1021/acs.energyfuels.9b00867
Energy Fuels XXXX, XXX, XXX−XXX

demonstrate that these high-resolution spectra depend on the substitution pattern of the porphyrin and that they can be used to identify types of porphyrins in a mixture. This provides a new avenue for separation-free speciation of vanadyl compounds in crude oil.

RESULTS AND DISCUSSION

For our study of the ligand structure of various vanadyl porphyrins, we utilized four commercially available vanadyl porphyrins. Their structures are shown in Figure 1, with color-coded chemically distinct protons. All porphyrins have an identical porphin core and differ only in the alkylation or arylation substitution patterns. Vanadyl octaethylporphyrin (VO-OEP) and vanadyl etioporphyrin (VO-EP) were chosen because they are among the most common naturally occurring petroporphyrins. In these ligands, the pyrrole hydrogens are all substituted with ethyl groups (OEP) or a mix of methyl and ethyl groups (EP), but the hydrogens at the four meso positions are preserved. Some petroporphyrins, such as VO-DPEP, have additional substituents at some of the porphyrin meso positions. To model porphyrins with meso substituents (reducing the number of meso protons), we use vanadyl tetraphenylporphyrin (VO-TPP; no meso protons) and vanadyl diphenylporphyrin (VO-DPP; two meso protons).[6,8]

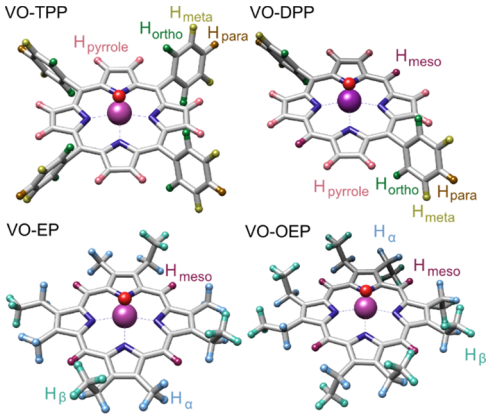

Figure 1. Vanadyl porphyrins investigated in this work. Chemically unique groups of protons are labeled and color-coded. The abbreviations are as follows: vanadyl tetraphenylporphyrin, VO-TPP; vanadyl diphenylporphyrin, VO-DPP; vanadyl etioporphyrin, VO-EP; vanadyl octaethylporphyrin, VO-OEP.

CW EPR. As mentioned in Introduction, the vanadyl ion VO^{2+} is paramagnetic with total electron spin 1/2. The single unpaired electron is located in a primarily d_{xy} orbital centered on the vanadium ion, with its four lobes in the porphyrin plane and pointing toward the porphyrin meso carbons.[30] A density functional theory (DFT) calculation (see Materials and Methods for details) of the spin density in VO-OEP is shown in Figure 2; the other vanadyl porphyrins give very similar results (not shown).

To probe the coupling between the delocalized unpaired electron and surrounding magnetic nuclei, we use CW EPR. The low-temperature X-band CW EPR spectrum for VO-OEP (black) along with a simulation (red) is shown in Figure 3 (top). The simulation parameters are listed in Table 1. The g-tensor and vanadium hyperfine tensor in the simulation are collinear and axial. As the g-tensor is essentially isotropic, the spectral features are primarily determined by the strongly

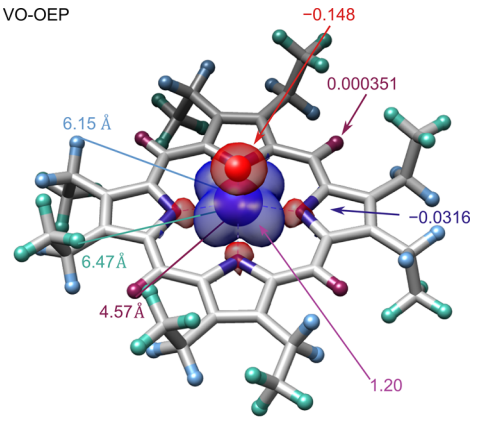

Figure 2. Calculated electron spin density of VO-OEP. The spin density contour level is drawn at ±0.002 electrons a_0^{-3}, and the positive and negative spin densities are colored blue and red, respectively. Values for magnetic nuclei with a Mulliken spin population >0.0001 and computationally predicted average values for vanadyl/proton distances are shown. The Mulliken spin populations of the pyrrole protons (not shown) have an average value of 0.00019.

anisotropic hyperfine splittings due to the coupling between the unpaired electron and the magnetic ^{51}V nucleus (99.75% natural abundance) with a nuclear spin of $I = 7/2$. The $2I + 1 = 8$ central features between 310 and 360 mT are due to porphyrins aligned such that the V−O direction is perpendicular (and the porphyrin plane is parallel) to the applied magnetic field.[31] The splittings that appear on both the high- and low-field sides of the central lines correspond to molecules oriented such that the V−O direction is parallel (and the porphyrin plane is perpendicular) to the magnetic field. The CW EPR spectra for the other compounds shown in Figure 3 are essentially identical to that of VO-OEP within experimental noise. The similarity of the spectra indicates that the spin density distribution around the vanadyl ion is independent of the nature of the porphyrin and that the magnetic environment is essentially unperturbed by changes in the substitution pattern on the porphyrin ligand. The hyperfine couplings to the magnetic nuclei of the porphyrin ligand (protons and nitrogens) are unresolved; the features are "buried" in the broad spectral features due to the large anisotropic ^{51}V hyperfine coupling. Therefore, CW EPR, although useful for quantifying the amount of vanadium, is incapable of differentiating vanadyl porphyrins. A technique with a higher resolution is required.

ENDOR. Porphyrin ligands differ in the number and location of protons. These can be determined from the hyperfine couplings between the protons and the central vanadyl ion, which are measurable using ^{1}H ENDOR spectroscopy. Pulsed ENDOR is a high-resolution EPR technique that allows a direct measurement of nuclear resonance frequencies in paramagnetic compounds and thereby provides access to hyperfine couplings. The coupling strength between an unpaired electron and a nucleus at position R is described by the hyperfine tensor A given by the equation

DOI: 10.1021/acs.energyfuels.9b00867
Energy Fuels XXXX, XXX, XXX−XXX

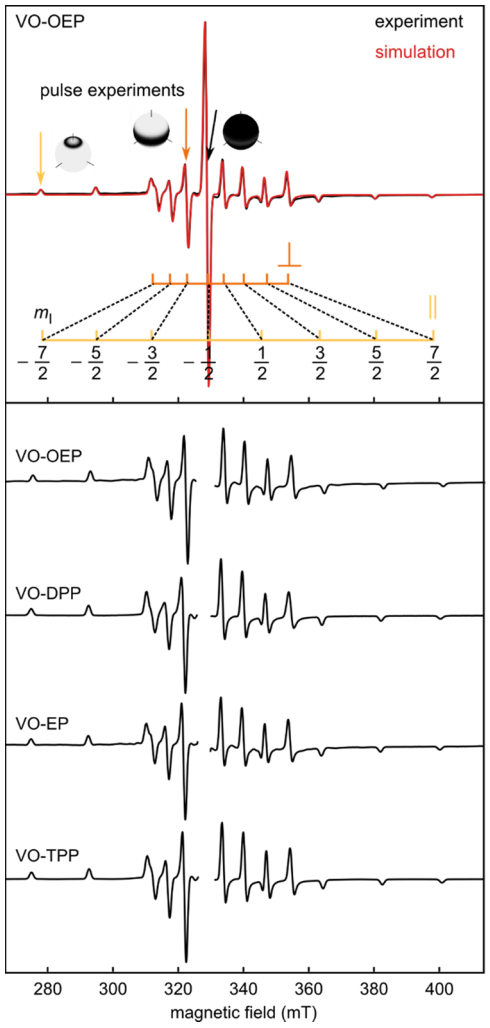

Figure 3. Top: X-band (9.297 GHz) CW EPR spectrum of 1 mM VO-OEP in 1:1 toluene-d_8/$CDCl_3$ (v/v) at 108 K. The simulation (red) is overlaid on the experimental trace (black). The ^{51}V nuclear spin manifolds are indicated for molecules with the field parallel and perpendicular to the V−O direction. The spectral positions and associated bandwidth of excitation (black) used for pulse experiments are indicated with arrows. Bottom: CW EPR spectra of the four model compounds with the central transition removed to allow for better comparison of the features with lower spectral intensity.

Table 1. EPR and ENDOR Simulation Parameters for the Model VO-Porphyrins[a]

g-tensor	g_x, g_y	g_z	frame ([α, β, γ]), °
	1.984(2)	1.964(2)	[0, 0, 0]
hyperfine tensors	T (MHz)	a_{iso} (MHz)	frame ([α, β, γ]), °
^{51}V	105(2)	263(3)	[0, 0, 0]
^1H meso	0.8(3)	0.5(3)	[0, 90(5), 0]
^1H pyrrole	0.56(4)	0.28(4)	[0, 90(5), 0]
^1H $ortho_{close}$	0.47(7)	[b]	[0, 55(10), 0]
^1H $ortho_{far}$	0.43(5)	[b]	[0, 55(10), 0]
^1H meta	0.16(2)	[b]	[0, 90(10), 0]
^1H alkyl 1	0.43(8)	[b]	[0, 60(15), 0]
^1H alkyl 2	0.32(5)	[b]	[0, 80(15), 0]
^1H alkyl 3	0.17(3)	[b]	[0, 45(15), 0]

[a]Not all ^1H are present in every compound. [b]Assumed to be zero.

$$A = \frac{2}{3h}\mu_0\mu_n g_n \mu_B g_e \rho^{\alpha-\beta}(R) + \frac{1}{4\pi h}\mu_0\mu_n g_n \mu_e g_e \left\langle \frac{3n\cdot n^T - \mathbf{I}}{r^3} \right\rangle \quad (1)$$

where h is Planck's constant, μ_0 is the magnetic constant, μ_n and μ_B are the nuclear and Bohr magneton, respectively, g_n and g_e are the nuclear and electron g values, respectively, $\rho^{\alpha-\beta}(R)$ is the spin density at the nucleus, n is a unit vector pointing from the unpaired electron to the nucleus, $\mathbf{I}$ is the 3 × 3 identity matrix, r is the distance between the unpaired electron and the nucleus, and the brackets indicate integration over the singly occupied molecular orbital (SOMO). The first term describes the Fermi contact coupling due to electron spin density at the nucleus position, and the second term describes the through-space coupling between the unpaired electron in the SOMO and magnetic nucleus. In the principal axis system of the hyperfine tensor, this relationship can be written in short as

$$A = a_{iso}\mathbf{I} + \begin{pmatrix} -T & 0 & 0 \\ 0 & -T & 0 \\ 0 & 0 & 2T \end{pmatrix} \quad (2)$$

where $a_{iso} = \frac{2}{3h}\mu_0\mu_n g_n \mu_B g_e \rho^{\alpha-\beta}(R)$ is the Fermi contact coupling constant, and $T = \frac{\mu_0\mu_n g_n \mu_B g_e}{4\pi h r^3}$ is the dipolar coupling constant.

The hyperfine interaction therefore contains information about the distance of protons from the vanadyl ion in the porphyrin compounds and the extent to which unpaired spin density is delocalized onto a proton. The latter is significant only for protons directly attached to the tetrapyrrole ring (meso and pyrrole hydrogens). Through the dipolar couplings, we can determine the distance distribution of protons from the vanadyl ion, which, in turn, allows us to differentiate the ligand structure of the individual vanadyl porphyrins. DFT calculations (vide infra) predict values of a_{iso} and T in the submegahertz range. To measure these small ^1H hyperfine couplings, we use the Mims ENDOR pulse sequence (see Materials and Methods).[32] The magnitude of the hyperfine couplings can be easily determined from a Mims ENDOR spectrum, as illustrated in Figure 4. The splitting between the inner peaks is equal to $|a_{iso} - T|$, and the overall width of the spectrum corresponds to $|a_{iso} + 2T|$. The full ENDOR spectrum is a sum of the ENDOR spectra from individual protons. However, spectral intensities in Mims ENDOR are subject to frequency-dependent suppression, with maximal suppression at frequency offsets of $n/2\tau$, where n is 0, ±1, ±2, ..., and τ is the time between the first two pulses in the pulse sequence. The central point (n = 0) is where the RF frequency equals the nuclear Larmor frequency. We chose τ = 150 ns such that the first pair of noncentral maximum suppression points ("blind spots") corresponding to n = ± 1 occur at ±3.3 MHz, outside the range of the spectra in this work.

The experimental ENDOR spectra for the model vanadyl porphyrins are shown in Figure 5. For each porphyrin, three ENDOR spectra acquired at the field positions indicated by arrows in Figure 3 are shown. The spectral shapes are distinct due to the varying types and numbers of protons in the model compounds. Figure 5 also shows simulations of the spectra. They are constructed by summing over simulations for each

DOI: 10.1021/acs.energyfuels.9b00867
Energy Fuels XXXX, XXX, XXX−XXX

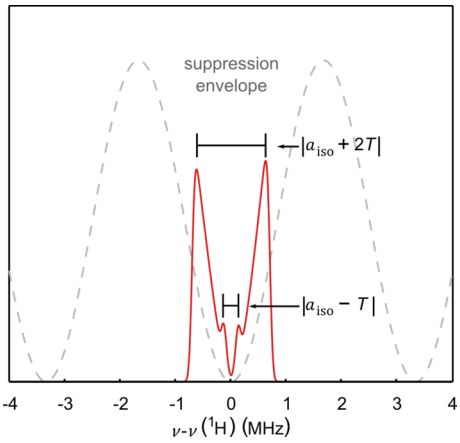

Figure 4. Simulated ^{1}H Mims ENDOR spectrum for interpreting spectral splitting. The simulation parameters are a_{iso} = 0.28 MHz and T = 0.56 MHz. The gray dashed line is the suppression envelope for a τ value of 150 ns, with maximal suppression at integer multiples of $1/2\tau \approx$ 3.3 MHz from the proton Larmor frequency $\nu(^1H)$.

unique group of protons in the model compounds. For each compound, the three ENDOR spectra were simulated using a single global parameter set. The best-fit results are listed in Table 1. Expected hyperfine parameters for each proton and each model compound were calculated using DFT (see Materials and Methods for details).

All features in the experimental spectra can be rationalized by comparison to the proton assignments in the simulation. The distinguishing features of the ENDOR spectra are primarily due to the dipolar couplings T, which are proportional to the inverse cube of the distance between the proton and unpaired electron spin density on the vanadium ion (see Equation 2 and Figure 4).

The hyperfine splitting with the largest magnitude is assigned to the meso protons. The associated spectral features are present in all spectra of compounds with meso protons (VO-DPP, VO-EP, VO-OEP) and are absent in VO-TPP, which does not have meso protons. The magnitude of the coupling is due to both through-space interactions and contact coupling. The meso protons are the protons closest to the unpaired electron and therefore have the largest through-space coupling (0.81 MHz, see Table 1). There is an additional 0.5 MHz contact coupling due to electron spin density directly on the meso protons (see Figure 2).

The next-largest splitting is attributed to the pyrrole protons. The features attributed to the pyrrole protons appear in the spectra for VO-DPP and VO-TPP and are absent in the spectra for VO-EP and VO-OEP, supporting the assignment. The coupling consists of a 0.56 MHz through-space dipolar component and a 0.28 MHz contact contribution. These values are reduced relative to the meso proton because the pyrrole protons are further away (r_{meso} = 4.47(5) Å, $r_{pyrrole}$ = 5.2(4) Å) from the vanadium ion and have lower electron spin density. The DFT calculations support the pyrrole assignment relatively well: Both the calculated pyrrole contact coupling (a_{iso} = 0.24 MHz) and the calculated dipolar coupling (T = 0.44 MHz) are just slightly smaller than the corresponding experimentally determined values.

The next features we assign are the phenyl protons in VO-TPP and VO-DPP. These protons have no measurable contact coupling, and the dipolar couplings are smaller than those of the meso and pyrrole protons because of their increased distance from vanadium. Additionally, based on crystal structures[33,34] and geometry calculations, the vanadyl ion sits slightly above the porphyrin plane, so the ortho and meta protons have different predicted coupling strengths based on whether they are on the proximal or distal side of the

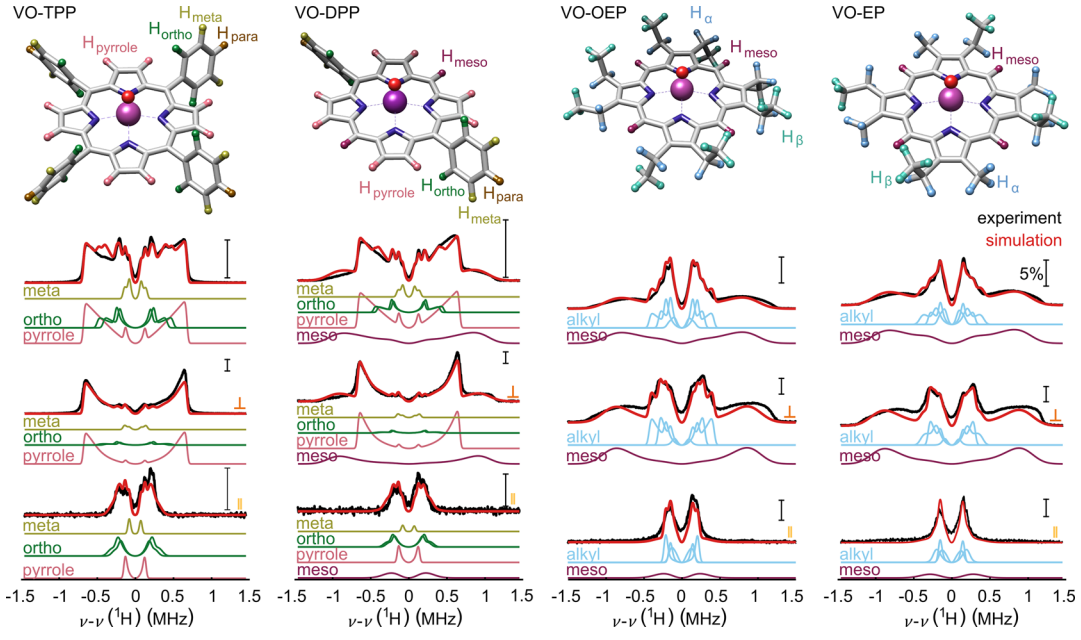

Figure 5. Experimental (black) and simulated (red) ENDOR spectra for each of the compounds in this work. Each compound is measured at three spectral positions probing orientation dependent features indicated in Figure 3: $m_I = -1/2$ (top, no orientation selection), ⊥ region of $m_I = -3/2$ (middle, orientation selection in xy plane), ∥ region of $m_I = -7/2$ (bottom, orientation selection along the z axis). Each simulated spectrum is obtained by simulating ENDOR spectra of individual protons (shown and labeled) and then summing them together. A black bar indicating 5% ENDOR efficiency is included for each spectrum. An offset is included for ease of visualization.

DOI: 10.1021/acs.energyfuels.9b00867
Energy Fuels XXXX, XXX, XXX−XXX

porphyrin plane relative to the vanadyl ion. Resolution of the ortho and meta hyperfine differences is challenging. The separation of the features assigned to the ortho protons is near the resolution limit of the experiment. The simulation is closer to the experimental results if two different ortho features are assumed (single ortho spectrum not shown), but the meta protons are assigned to a single distance because the resolution of the spectrum is insufficient to support a two-component fit. No features from the para protons are resolved. DFT predicts $T \approx 0.1$ MHz for them. The associated features lie very close to the Larmor frequency, and this region of the spectrum is strongly suppressed due to the central blind spot.

The final two types of protons are the alkyl protons in the methyl (α protons) and ethyl (α and β protons) groups in VO-OEP and VO-EP. Due to the distribution of dihedral angles, the α and β protons in the methyl and ethyl groups have overlapping distance distributions (to the vanadium), which leads to similar hyperfine couplings. Unfortunately, due to this distribution overlap, the assignment of α or β protons remains ambiguous. The simulation instead includes three distinct alkyl proton features that successfully model the features assigned to the α and β protons. Despite the overlap, the number and types of protons leads to qualitative differences in the alkyl region of the spectra of VO-OEP and VO-EP.

The presence or absence of spectral features in the ENDOR spectra in Figure 5 allows the classification of the porphyrin ligand. The most obvious features to assign are the protons directly attached to the porphyrin ring. The meso and pyrrole protons have unique and distinguishable spectra. Therefore, the presence/absence of meso or pyrrole protons is immediately clear from the ENDOR spectra, allowing the identification of the ring substitution pattern. For example, comparing the spectra for VO-TPP and VO-OEP in Figure 5, the absence of meso protons in VO-TPP results in a spectrum that is ≈1 MHz narrower and does not feature broad peaks at ±1 MHz. Without a pyrrole feature, the overall VO-OEP spectrum does not narrow, but the intense features at ±0.7 MHz disappear. The ligand protons are not directly quantifiable; however, some semiquantitative statements can be made. Comparing the intensities of the lines from the substituent protons to the ones from the porphyrin ring protons offers some insight into the number of protons in the alkyl or aryl substituents. For example, by comparing VO-OEP and VO-EP, the intensity of the central features relative to the meso wings reveals that VO-OEP has a larger number of weakly coupled ligand protons than VO-EP.

Via the dipolar couplings, ENDOR yields an experimental measurement of the distances of ligand protons from the vanadyl ion. A comparison of our ENDOR findings with computed distances based on DFT calculations and experimental distances from crystal structures of vanadyl porphyrin compounds[33,34] is shown in Figure 6. As demonstrated in the figure, ENDOR successfully captures the distribution of protons that are located between 4.5 and 8 Å from the vanadyl ion. Even at the low-distance end of this range, it appears that the point-dipole approximation (i.e., assuming the SOMO spin population on vanadyl to be localized at the vanadium nucleus) is reasonably accurate. For higher accuracy, the spatial extent of the SOMO must be taken into account more explicitly near this short-distance limit. The long-distance limit of about 8 Å is primarily due to a lack of spectral resolution and the low intensity due to the Mims ENDOR suppression envelope. The protons in the most common

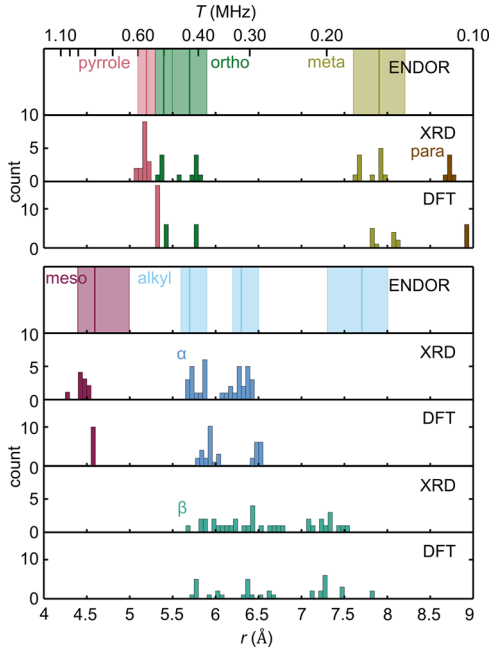

Figure 6. Distance distribution of protons in the vanadyl porphyrins VO-TPP, VO-DPP, VO-EP, and VO-OEP determined from ENDOR spectra, X-ray crystal structures, and DFT calculations. Top: pyrrole and phenyl protons. Bottom: meso and alkyl protons. The magnitude of the dipolar hyperfine coupling as a function of distance is given as a second horizontal axis along the top of the figure.

petroporphyrins fall within the 4.5−8 Å distance range accessible by high-resolution ENDOR.

The significant differences among the observed ENDOR spectra of vanadyl porphyrins suggest that it could be possible to differentiate them within mixtures. To test this, we prepared mixtures of VO-EP/VO-OEP and of VO-TPP/VO-OEP. We then used linear combinations of simulated pure-compound spectra to construct new simulations that fit the mixture spectra by least-squares fitting. The results are shown in Figure 7. The error bars represent one standard deviation of the best-fit parameter. The difference in magnitude of the error bars is directly related to the relative differences of the pure compound spectra. The ENDOR spectra of VO-OEP and VO-EP are very similar; therefore, as the relative concentration between the two compounds change, the overall spectrum does not significantly change. On the other hand, the spectral difference between VO-OEP and VO-TPP is more significant. For example, as the relative concentration of VO-TPP increases, the spectral features due to the pyrrole protons become more intense, and simultaneously, the features due to meso protons decrease. These larger differences lead to smaller best-fit parameter uncertainties. Figure 7 shows that it is possible to determine the composition of porphyrins in a binary mixture with reasonable accuracy and precision. Remarkably, even vanadyl porphyrins as similar as VO-OEP and VO-EP are quantitatively distinguishable within a mixture.

CONCLUSIONS

We have shown that EPR is a useful tool for classifying vanadyl porphyrins. With high-resolution ^{1}H ENDOR spectroscopy, we could clearly differentiate ligands in model vanadyl porphyrins via ligand proton (super)hyperfine couplings. The high spectral resolution allowed us to distinguish features due

DOI: 10.1021/acs.energyfuels.9b00867
Energy Fuels XXXX, XXX, XXX−XXX

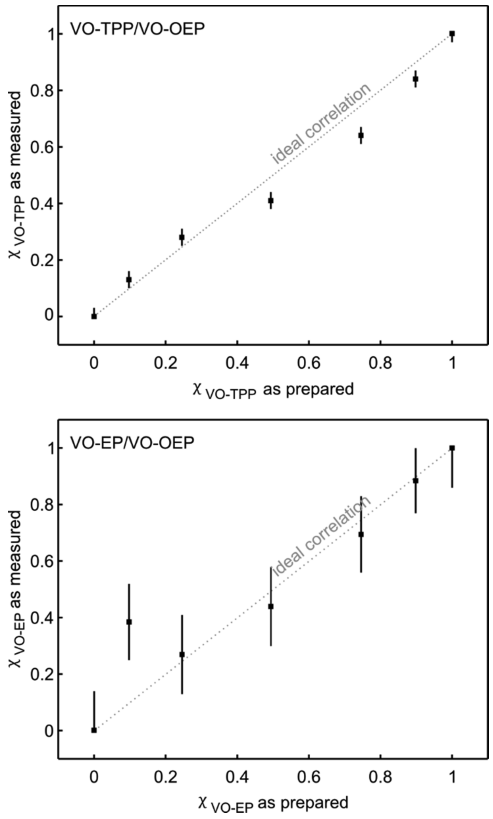

Figure 7. Comparison of measured compositions versus prepared compositions of binary mixtures of vanadyl porphyrins. Top: VO-TPP/VO-OEP mixtures. (b) VO-EP/VO-OEP mixtures. χ indicates the molar fraction of the compound in its subscript. The vertical error bars correspond to the standard deviation of the best-fit parameter. Horizontal error bars are negligible on the scale of the plot. Gray dashed line: ideal correlation.

to protons with a difference in hyperfine coupling as small as 0.15 MHz and to determine distances between the electron spin on vanadium and protons in the range 4.5−8 Å. We found that couplings of protons in equivalent positions are similar across different porphyrin compounds. The ENDOR-based method introduced in this work directly reveals the substitution pattern on the tetrapyrrole ring (meso and pyrrole positions), something that is not possible with other methods. ENDOR also provides insight into the number of protons on the aryl or alkyl substituents. Finally, we demonstrated that the composition of mixtures of vanadyl porphyrins can be determined. This methodology is therefore potentially useful for the speciation of vanadyl porphyrin ligands in crude oils. Such samples will have two potential complications: (1) The ENDOR spectra will feature additional signals from remote matrix protons. However, they are centered in a narrow region around the Larmor frequency and will therefore not interfere strongly with the detection and assignment of porphyrin protons. (2) The samples are more complex mixtures as they will contain more than just two vanadyl porphyrins. In this situation, the ENDOR methodology will not allow speciation of every single component but will still be able to measure the ring substitution pattern and relative content of ring and substituent protons, allowing a broad classification of porphyrin ligands.

MATERIALS AND METHODS

All vanadyl complexes were purchased from Frontier Scientific. The deuterated solvents were obtained from Cambridge Isotope Laboratories. Samples were prepared with ≈1 mM concentration in 1:1 (v/v) toluene-d_8/$CDCl_3$, filled into 4 mm o.d. quartz tubes and flash-frozen by immersion into liquid nitrogen.

CW EPR. The CW EPR data were measured with a Bruker EMX spectrometer equipped with a Bruker SHQE resonator. The experimental sample temperature was between 107 and 110 K, and the resonator Q factor was ≈4700. The modulation frequency and amplitude were set to 100 kHz and 0.5 mT, respectively, the scan rate was 1.7 mT s^{-1}, and the microwave power was 158 μW.

Pulse EPR. All pulse EPR data were measured at X-band with a Bruker Elexsys E580 spectrometer equipped with a Bruker MD4 dielectric resonator with broadband ENDOR coils. The microwave power was amplified with a 1 kW amplifier, and RF power was provided by a 250 W amplifier. Pulse experiments were performed at fields corresponding to the $m_I = -1/2, -3/2, -7/2$ features of the vanadyl spectrum. These spectral positions allow probing of minimal, perpendicular, and parallel orientation selection, respectively (see Figure 3). The Mims ENDOR[32] data were collected at 42 K for all pure compounds and mixtures. The value of τ was 150 ns, and the microwave pulses were all 12 ns long. An RF pulse length of 30 μs (corresponding to a spectral excitation window width of about 0.04 MHz) was chosen to minimize RF power broadening on the narrow ENDOR spectra. Shorter RF pulses lead to power broadening, and longer pulses lead to loss of ENDOR signal. The power required for the 30 μs-long π RF pulse was 12.5 W. The shot repetition time was 3 ms. ENDOR spectra are slightly asymmetric due to the variation of the RF pulse flip angle over the spectral range, which is a consequence of hyperfine enhancement. We refrained from symmetrizing the spectra. The experiments were run at X-band (ca. 9.5 GHz, 0.3 T) instead of Q-band (35 GHz, 1.2 T) due to strong cross-suppression[35] of the ^{1}H peak from the pyrrole ^{14}N nitrogens at Q-band.

Simulations. All CW EPR and ENDOR spectral simulations were performed using EasySpin 5.2.[36] Values from DFT calculations were used as the starting values for the simulations. The simulation parameters were refined manually until the simulations recreated the experimental spectra. The varied CW spectral parameters were an axial g-tensor, an axial hyperfine tensor, and Voigtian broadening. The ENDOR spectral parameters were a contact coupling term a_{iso}, a dipolar coupling term T, an angular term defining the orientation of the hyperfine tensor frame relative to the molecular frame, and the relative intensity among individual proton features.

DFT. DFT calculations for initial estimates of magnetic parameters (g, hyperfine, and quadrupole tensors) were performed using ORCA 3.0.3.[37] For each compound, geometry optimization was performed with the BP86 functional[38,39] and the def-svp[40] basis set along with the def-svp/j[41] basis set for all atoms. The integration grid and convergence criteria were set to 3 and tight, respectively. The predicted magnetic properties for each compound including g values, all nuclear hyperfine couplings, and nuclear quadrupole couplings were calculated using ORCA by starting with the optimized geometry and utilizing the B3LYP functional,[38,42−45] the EPR-II basis set[46] for all atoms except vanadium, and the CP(PPP) basis set[47] for vanadium to better represent the electron density near the vanadium nucleus. The integration grid and convergence criteria were set to 7 and tight, respectively. The resulting parameters from the DFT calculations were used as starting points for the spectral simulations.

Geometries. The DFT distances in Figure 6 were taken from the optimized geometry of each structure. The crystal distances were taken from reported structures for VO-OEP[34] and VO-EP.[33] Data were collected and structures were determined for crystals of VO-TPP and VO-DPP grown in THF at −173 °C on a Bruker APEX II single-crystal X-ray diffractometer using a Mo tube.

AUTHOR INFORMATION

Corresponding Author

*E-mail: stst@uw.edu.

DOI: 10.1021/acs.energyfuels.9b00867
Energy Fuels XXXX, XXX, XXX−XXX

ORCID

Stefan Stoll: 0000-0003-4255-9550

Author Contributions

D.M. and S.S. planned the experiments. D.M. performed and analyzed the experiments. D.M. and S.S. wrote the manuscript. All authors have given approval to the final version of the manuscript.

Notes

The authors declare no competing financial interest.

■ ACKNOWLEDGMENTS

This work was, in part, funded by the ACS Petroleum Research Fund (grant 54860-DNI4 to S.S.) and by the NSF (CHE-1452967 to S.S.). We thank Werner Kaminsky for the acquisition of the X-ray structures.

■ ABBREVIATIONS

VO-TPP = vanadyl tetraphenylporphyrin
VO-DPP = vanadyl diphenylporphyrin
VO-EP = vanadyl etioporphyrin
VO-OEP = vanadyl octaethylporphyrin
EPR = electron paramagnetic resonance
CW = continuous wave
ENDOR = electron nuclear double resonance
DFT = density functional theory
SOMO = singly occupied molecular orbital
DPEP = deoxophylloerythroetioporphyrin
FT-ICR MS = Fourier-transform ion cyclotron resonance mass spectrometry

■ REFERENCES

(1) Larocca, M.; De Lasa, H.; Farag, H.; Ng, S. *Ind. Eng. Chem. Res.* **1990**, *29*, 2181−2191.
(2) Pearson, C. D.; Green, J. B. *Energy Fuels* **1993**, *7*, 338−346.
(3) Marques, J.; Guillaume, D.; Merdrignac, I.; Espinat, D.; Brunet, S. *Appl. Catal., B* **2011**, *101*, 727−737.
(4) Lepri, F. G.; Welz, B.; Borges, D. L. G.; Silva, A. F.; Vale, M. G. R.; Heitmann, U. *Anal. Chim. Acta* **2006**, *558*, 195−200.
(5) Kim, C.-S.; Massoth, F. E. *Fuel Process. Technol.* **1993**, *35*, 289−302.
(6) McKenna, A. M.; Purcell, J. M.; Rodgers, R. P.; Marshall, A. G. *Energy Fuels* **2009**, *23*, 2122−2128.
(7) Dunning, H. N.; Moore, J. W.; Bieber, H.; Williams, R. B. *J. Chem. Eng. Data* **1960**, *5*, 546−549.
(8) Gilinskaya, L. G. *J. Struct. Chem.* **2008**, *49*, 245−254.
(9) Premović, P. I.; Allard, T.; Nikolić, N. D.; Tonsa, I. R.; Pavlović, M. S. *Fuel* **2000**, *79*, 813−819.
(10) Gerfen, G. J.; Hanna, P. M.; Chasteen, N. D.; Singel, D. J. *J. Am. Chem. Soc.* **1991**, *113*, 9513−9519.
(11) Saraceno, A. J.; Fanale, D. T.; Coggeshall, N. D. *Anal. Chem.* **1961**, *33*, 500−505.
(12) Galtsev, V. E.; Ametov, I. M.; Grinberg, O. Y. *Fuel* **1995**, *74*, 670−673.
(13) Biktagirov, T.; Gafurov, M.; Mamin, G.; Gracheva, I.; Galukhin, A.; Orlinskii, S. *Energy Fuels* **2017**, 1243.
(14) Mamin, G. V.; Gafurov, M. R.; Yusupov, R. V.; Gracheva, I. N.; Ganeeva, Y. M.; Yusupova, T. N.; Orlinskii, S. B. *Energy Fuels* **2016**, *30*, 6942−6946.
(15) Ben Tayeb, K.; Delpoux, O.; Barbier, J.; Marques, J.; Verstraete, J.; Vezin, H. *Energy Fuels* **2015**, *29*, 4608−4615.
(16) Dechaine, G. P.; Gray, M. R. *Energy Fuels* **2010**, *24*, 2795−2808.
(17) Zhao, X.; Xu, C.; Shi, Q. Porphyrins in Heavy Petroleums: A Review. In *Structure and Modeling of Complex Petroleum Mixtures. Structure and Bonding*; Xu, C., Shi, Q., Eds.; Springer: Cham, 2015; vol *168*.
(18) Dunning, H. N.; Rabon, N. A. *Ind. Eng. Chem.* **1956**, *48*, 951−955.
(19) Benamsili, L.; Korb, J. P.; Hamon, G.; Louis-Joseph, A.; Bouyssiere, B.; Zhou, H.; Bryant, R. G. *Energy Fuels* **2014**, *28*, 1629−1640.
(20) Barwise, A. J. G. *Energy Fuels* **1990**, *4*, 647−652.
(21) Goulon, J.; Retournard, A.; Friant, P.; Goulon-Ginet, C.; Berthe, C.; Muller, J.-F.; Poncet, J.-L.; Guilard, R.; Escalier, J.-C.; Neff, B. *J. Chem. Soc., Dalton Trans.* **1984**, 1095−1103.
(22) Qian, K.; Mennito, A. S.; Edwards, K. E.; Ferrughelli, D. T. *Rapid Commun. Mass Spectrom.* **2008**, *22*, 2153−2160.
(23) McKenna, A. M.; Williams, J. T.; Putman, J. C.; Aeppli, C.; Reddy, C. M.; Valentine, D. L.; Lemkau, K. L.; Kellermann, M. Y.; Savory, J. J.; Kaiser, N. K.; Marshall, A. G.; Rodgers, R. P. *Energy Fuels* **2014**, *28*, 2454−2464.
(24) Kivelson, D.; Lee, S.-K. *J. Chem. Phys.* **1964**, *41*, 1896−1903.
(25) Trukhan, S. N.; Kazarian, S. G.; Martyanov, O. N. *Energy Fuels* **2017**, *31*, 387−394.
(26) Volodin, M. A.; Mamin, G. V.; Izotov, V. V.; Orlinskii, S. B. *J. Phys.: Conf. Ser.* **2013**, *478*, No. 012003.
(27) Mustafi, D.; Telser, J.; Makinen, M. W. *J. Am. Chem. Soc.* **1992**, *114*, 6219−6226.
(28) Gourier, D.; Delpoux, O.; Bonduelle, A.; Binet, L.; Ciofini, I.; Vezin, H. *J. Phys. Chem. B* **2010**, *114*, 3714−3725.
(29) Mulks, C. F.; Van Willigen, H. *J. Phys. Chem.* **1981**, *85*, 1220−1224.
(30) Ballhausen, C. J.; Gray, H. B. *Inorg. Chem.* **1962**, *1*, 111−122.
(31) Mustafi, D.; Makinen, M. W. *Inorg. Chem.* **2005**, *44*, 5580−5590.
(32) Mims, W. B. *Proc. R. Soc. A* **1965**, *283*, 452−457.
(33) Drew, M. G. B.; Mitchell, P. C. H.; Scott, C. E. *Inorg. Chim. Acta* **1984**, *82*, 63−68.
(34) Molinaro, F. S.; Ibers, J. A. *Inorg. Chem.* **1976**, *15*, 2278−2283.
(35) Stoll, S.; Calle, C.; Mitrikas, G.; Schweiger, A. *J. Magn. Reson.* **2005**, *177*, 93−101.
(36) Stoll, S.; Schweiger, A. *J. Magn. Reson.* **2006**, *178*, 42−55.
(37) Neese, F. *Wiley Interdiscip. Rev.: Comput. Mol. Sci.* **2012**, *2*, 73−78.
(38) Becke, A. D. *Phys. Rev. A* **1988**, *38*, 3098.
(39) Perdew, J. P. *Phys. Rev. B* **1986**, *33*, 8822−8824.
(40) Schäfer, A.; Horn, H.; Ahlrichs, R. *J. Chem. Phys.* **1992**, *97*, 2571−2577.
(41) Schäfer, A.; Huber, C.; Ahlrichs, R. *J. Chem. Phys.* **1994**, *100*, 5829.
(42) Stephens, P. J.; Devlin, F. J.; Chabalowski, C. F.; Frisch, M. J. *J. Phys. Chem.* **1994**, *98*, 11623−11627.
(43) Lee, C.; Yang, W.; Parr, R. G. *Phys. Rev. B* **1988**, *37*, 785−789.
(44) Becke, A. D. *J. Chem. Phys.* **1993**, *98*, 5648.
(45) Becke, A. D. *J. Chem. Phys.* **1993**, *98*, 1372.
(46) Rega, N.; Cossi, M.; Barone, V. *J. Chem. Phys.* **1996**, *105*, 11060−11067.
(47) Neese, F. *Inorg. Chim. Acta* **2002**, *337*, 181−192.

DOI: 10.1021/acs.energyfuels.9b00867
Energy Fuels XXXX, XXX, XXX−XXX